IMMUNOLOGY

LPS binding caspase activation and recruitment domains (CARDs) are bipartite lipid binding modules

Anh B. Cao[1], Pascal Devant[1], Chengliang Wang[2], Mengyu Sun[1], Stephanie N. Kennedy[1], Weiyi Ma[1], Jianbin Ruan[2], Jonathan C. Kagan[1]*

Caspase-11 is an innate immune pattern recognition receptor (PRR) that detects cytosolic bacterial lipopolysaccharides (LPS) through its caspase activation and recruitment domain (CARD). Caspase-11 also detects eukaryotic (i.e., self) lipids. This observation raises the question of whether common or distinct mechanisms govern caspase interactions with self- and nonself-lipids. In this study, using biochemical, computational, and cell-based assays, we report that the caspase-11 CARD functions as a bipartite lipid-binding module. Distinct regions within the CARD bind to phosphate groups and long acyl chains of self- and nonself-lipids. Self-lipid binding capability is conserved across numerous caspase-11 homologs and orthologs. The symmetry in self- and nonself-lipid detection mechanisms enabled us to engineer an LPS-binding domain de novo, using an ancestral CARD-like domain present in the fish *Amphilophus citrinellus*. These findings offer insights into the molecular basis of LPS recognition by caspase-11 and highlight the fundamental and likely inseparable relationship between self and nonself discrimination.

INTRODUCTION

The accuracy of self-nonself discrimination is central to organismal identity and host defense. Within mammals, these two needs are not distinct, as the accurate identification of self-molecules is key for immune system functions in host defense. This "self-first" paradigm was uncovered through studies of how antigen receptor interactions affect lymphocyte development (*1*). In the thymus, developing T cells are first selected for the expression of α/β T cell receptors (TCRs) that recognize self-peptides associated with major histocompatibility complex (*1*, *2*). T cells bearing self-reactive TCRs are subsequently subjected to negative selection to eliminate cells that react excessively to self-components. Only after this process is complete do T cells exit the thymus to survey the body for nonself-antigens (*1*, *2*).

In contrast to the self-first paradigm of lymphocyte functions, the functions of myeloid cells are considered to operate via the opposite principle to govern host defense. Rather than detecting self-molecules, macrophages and dendritic cells, for example, use pattern recognition receptors (PRRs) to identify nonself-molecules such as microbial cell wall components or nucleic acids (*3*). These PRR ligands are referred to as pathogen associated molecular patterns (PAMPs). The germline encoded nature of genes encoding PRRs has led to the belief that PRRs are fixed in their specificity within a given species, whereas each organism has a unique antigen receptor repertoire (*3*). However, PRRs are among of the most rapidly evolving proteins in nature, suggesting that PRR specificity remains subject to evolutionary pressures (*4*, *5*). Such pressures are commonly discussed in the context of infection, whereby PRRs need to evolve to maintain the ability to detect pathogens that have higher rates of mutation and faster replication cycles (*4*, *5*).

The above-described selective pressure relates to the need for a PRR to detect nonself, to ensure efficient pathogen detection. Another pressure on PRRs could be the need to avoid the detection of self, to prevent pathological inflammatory responses in the absence of infection. In this view, self-ligand detection would be an activity that is counter selected for PRRs, but positively selected in antigen receptors. Yet, instances of self-ligand detection by PRRs are increasingly common. For example, while nucleic acids are not uniquely nonself-molecules, DNA and RNA structures are the most common PAMPs in humans and mice (*3*). Nucleic acid–sensing PRRs include 5 of the 12 members of the murine Toll-like receptor (TLR) family, all three members of the RIG-I–like receptor family, and the PRRs protein kinase R, absent in melanoma 2 (AIM2), and cyclic guanosine monophosphate–adenosine monophosphate synthase (*6*–*8*) As there is no feature of microbial nucleic acids that provides a definitive distinction from self-nucleic acids (*6*, *9*–*12*), it is puzzling why the most common PAMPs offer such a blurry line between self and nonself. Stated differently, if self-detection activities were counterselected for during PRR evolution, then nucleic acids would not have evolved as the most common type of PAMP.

The best justification that self-ligand detection is a counterselected trait relates to PRRs that detect cell wall components. The complex biochemical mechanisms that build a microbial cell are not encoded by mammalian genomes, leading to cell wall components being considered PAMPs with no self-equivalent. Yet, even for PRRs that detect cell wall components, self-ligands have been reported. For example, the PRRs CD14, TLR4, MD-2, and caspase-11 reportedly bind a collection of oxidized phosphatidylcholines (oxPAPCs) that are produced by injured or dying mammalian cells (*13*–*16*). Discussing the differences between self- and nonself-detection mechanisms by cell wall–sensing PRRs is mainly a philosophical exercise, as we lack biochemical insight into how these receptor-ligand interactions occur.

In this study, we used the lipopolysaccharide (LPS) and oxPAPC receptor caspase-11 as a model to define the mechanisms of self- versus nonself-detection. We discovered that despite their diversity of source, self- and nonself-lipids use a common mechanism to interact with caspase-11. This mechanism was defined at the level of the lipid and the ligand binding domain. The symmetry of mechanisms of interaction between self- and nonself-lipids extended to

[1]Division of Gastroenterology, Boston Children's Hospital, Harvard Medical School, 300 Longwood Avenue, Boston, MA 02115, USA. [2]Department of Immunology, UConn Health School of Medicine, 263 Farmington Ave., Farmington, CT 06030, USA.
*Corresponding author. Email: jonathan.kagan@childrens.harvard.edu

numerous caspase-11 homologs in distinct species of animals, knowledge of which enabled the derivation of an LPS receptor de novo. These findings reveal the molecular pattern present in LPS and self-lipids that is detected by caspase-11, and highlight self-ligand recognition as a (perhaps) unavoidable aspect of PRR activities.

RESULTS

Distinct biochemical activities mediate caspase-11 binding and aggregation

Caspase-11 aggregation has served as an indicator of its interaction with LPS (*17*). This assay, however, has limitations, as LPS from *Rhodobacter sphaeroides* (LPS-RS) binds with high affinity to caspase-11 but does not induce aggregation (*17*). We verified these findings, as LPS-RS failed to induce caspase-11 aggregation on native polyacrylamide gel electrophoresis (PAGE) (Fig. 1A). To detect nonaggregating caspase-11 binding events, we used a competitive assay to inhibit caspase-11 aggregation in the presence of LPS from *Escherichia coli* (LPS-EB; serotype O111:B4) and other competitive ligands. Co-incubation of caspase-11 with LPS-EB in the presence of increasing concentrations of LPS-RS hindered caspase-11 aggregation in this assay (Fig. 1A). As expected (*17*), caspase-11 CARD alone demonstrated the ability to aggregate upon binding LPS-EB (Fig. 1B).

Like LPS, oxPAPC is a heterogenous mixture of lipids, which complicates biochemical interaction studies with caspase-11. Within the oxPAPC mixture of self-lipids is a chemically defined and soluble entity known as PGPC (1-palmitoyl-2-glutaryl phosphatidylcholine) (*16*). To determine whether PGPC forms direct contacts with caspase-11, similar biochemical analyses were performed. We found that PGPC did not induce caspase-11 aggregation, as assessed by native PAGE, but PGPC inhibited LPS-induced caspase-11 aggregation (Fig. 1C). Muramyl dipepeptide (MDP), a PAMP that does not interact with caspase-11 (*17*), did not affect LPS-induced caspase-11 aggregation (Fig. 1, B to D). PGPC may therefore bind caspase-11.

To investigate whether the interaction between caspase-11 and its ligands alters the protein's secondary structure, we measured the circular dichroism (CD) spectra of recombinant full-length caspase-11 in the absence and presence of various ligands, including MDP, LPS-EB, LPS-RS, and PGPC. Caspase-11 alone exhibited a CD spectrum characteristic of a predominantly α-helical structure. This profile shifted further toward an α-helical conformation in the presence of the nonaggregating ligands LPS-RS and PGPC (Fig. 1D). LPS-EB also induced a shift toward a more α-helical structure; however, the shift was less pronounced compared to LPS-RS and PGPC. The aggregation of caspase-11 induced by LPS-EB may have complicated direct comparisons with the nonaggregating ligands. MDP treatment caused minimal changes in caspase-11 secondary structure (Fig. 1D).

Consistent with the spectral analysis, deconvolution of the CD spectra revealed that LPS-RS and PGPC significantly altered caspase-11's secondary structure by increasing the proportion of α-helices while reducing the "others" category, which includes unidentified or disordered structures. Conversely, MDP caused no significant changes to the secondary structure of caspase-11 (Fig. 1E). LPS and PGPC are therefore both capable of inducing a helical state of caspase-11.

An aggregation-independent assay to monitor lipid–caspase-11 interactions

On the basis of the CD analysis, we reasoned that caspase-lipid interactions would alter molecular conformations in a manner that reveals or obstructs protease cleavage sites. As such, limited trypsin digestion was used as a proxy for evaluating the interaction between caspase-11 and its ligands. Changes in molecular conformation may result in ligand-dependent tryptic digestion patterns that would be identified via immunoblot analysis (Fig. 2A). This assay would therefore use differential tryptic cleavage, rather than protein aggregation, as a readout of protein-lipid interactions.

When exposed to trypsin, full-length (45-kDa) caspase-11 present within cell lysates underwent degradation within 15 min, yielding a 20-kDa fragment that was evident by immunoblot analysis (Fig. 2B). In the presence of LPS-EB, caspase-11 exhibited a distinct state of trypsin resistance, resulting in the emergence of a higher molecular weight band (35 kDa) (Fig. 2B). Similarly, LPS-RS and PGPC, which bind but do not aggregate caspase-11, exhibited similar banding patterns as LPS-EB during limited trypsin digestion (Fig. 2B).

In contrast to the lipid-induced protection of caspase-11 to protease cleavage, the tryptic digestion patterns of caspase-3 and β-tubulin were unaffected by LPS-EB, LPS-RS, or PGPC (Fig. 2B). In addition, no alteration of intrinsic trypsin enzymatic activity (as assessed by spectrofluorimetry) was observed in the presence of lipids (Fig. 2C). To assess the specificity of the trypsin resistance assay to report on caspase-ligand interactions, we examined caspase-11 cleavage in the presence of microbial products that are reported to not bind caspase-11 (*17*). In the limited trypsin digestion assay, we investigated the effect of various PAMPs including MDP, Polyinosinic-polycytidylic acid [Poly(I:C)], Poly(deoxyadenylic-deoxythymidylic) acidPoly(dA:dT), L-Ala-γ-D-Glu-mDAP (Tri-DAP), bis-(3′-5′)-cyclic dimeric adenosine monophosphate (c-di-AMP), cyclic guanosine monophosphate–adenosine monophosphate (cGAMP), and peptidoglycan (PGN). None of these microbial products influenced the tryptic digestion of caspase-11 (Fig. 2D).

To identify the regions of caspase-11 protected from tryptic digestion upon lipid binding, we conducted similar studies using recombinant caspase-11, followed by mass spectrometry. This analysis revealed that the 20-kDa band lacked peptides preceding K62, whereas the 35-kDa band retained the same N-terminal composition as the undigested full-length protein (Fig. 2E). Notably, K62 resides within the CARD of caspase-11. Both the 35-kDa band (present only upon ligand binding) and the 20-kDa band (present in the absence of ligand) lacked peptides C-terminal to R265 (Fig. 2E). These data suggest that binding of LPS or PGPC induces a common conformational change in the CARD that transforms it from a trypsin-sensitive to an α-helical trypsin-resistant state. Consistent with this idea, we found that PGPC prevented LPS-induced aggregation of the CARD of caspase-11 (Fig. 2F). In addition, liquid chromatography revealed that the caspase-11 CARD eluted in an earlier fraction in the presence of PGPC compared to caspase-11 CARD alone (Fig. 2G). This shift in elution profile suggests a stable complex is formed between PGPC and the caspase-11 CARD. Microscale thermophoresis (MST) was used to quantify the binding affinity between PGPC and the CARD, resulting in a determined K_d value of approximately 15 μM (Fig. 2H). As the binding affinity between the caspase-11 CARD and PGPC is lower than the critical micelle concentration of PGPC (~50 μM) (*18*), the CARD of caspase-11 may have the capacity to interact with PGPC monomers.

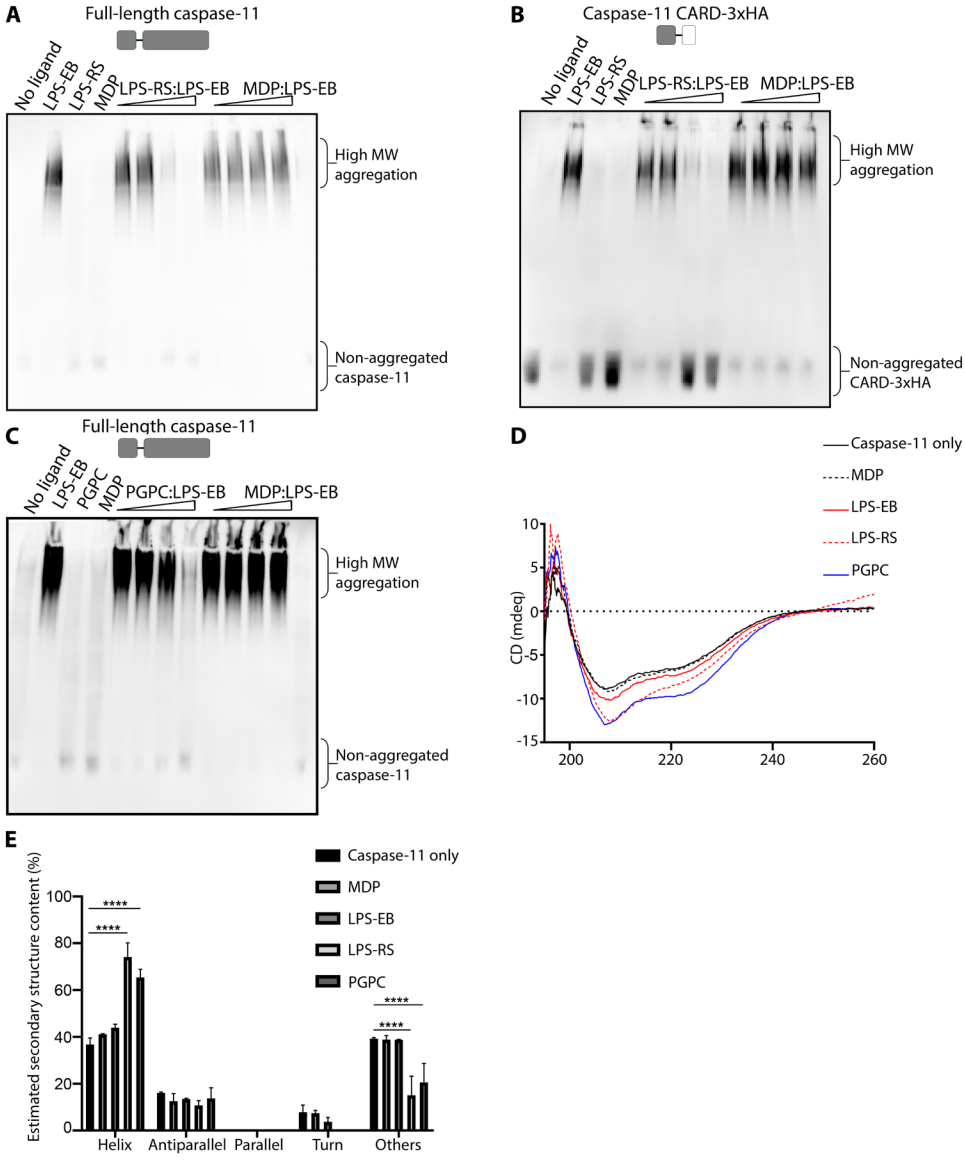

Fig. 1. Caspase-11 CARD binds to monoacylated PGPC without aggregation. (**A**) 293 T cell lysates expressing exogenous full-length caspase-11 were incubated at room temperature for 30 min with LPS-EB, LPS-RS, muramyl dipeptide (MDP), or combinations thereof. Protein complexes were resolved by blue native gel electrophoresis and analyzed via immunoblotting to detect caspase-11. (**B**) 293T cell lysates expressing HA-tagged caspase-11 CARD domain were incubated at room temperature for 30 min with LPS-EB, LPS-RS, MDP, or combinations thereof. Protein complexes were resolved by blue native gel electrophoresis and analyzed via immunoblotting to detect HA tag. (**C**) 293T cell lysates expressing exogenous full-length caspase-11 were incubated at room temperature for 30 min with LPS-EB, PGPC, MDP, or combinations thereof. Protein complexes were resolved by blue native gel electrophoresis and analyzed via immunoblotting to detect caspase-11. (**D**) The circular dichroism (CD) spectra of recombinant full-length caspase-11 (0.1 mg/ml) were measured in the absence or presence of various ligands, including MDP (100 μg/ml), LPS-EB (100 μg/ml), LPS-RS (100 μg/ml), and PGPC (100 μg/ml). (**E**) Quantitative analysis of caspase-11 secondary structure content based on CD spectra deconvolution analyzed by BESTSEL. Data are from of three independent experiments, and results with error bars are presented as means ± SEM. Statistical significance was determined by an ordinary two-way ANOVA compared to caspase-11 alone. ns = not significant; *$P < 0.05$, **$P < 0.01$, ***$P < 0.001$, and ****$P < 0.0001$.

Caspase-11 binds lipids with diverse headgroup chemistries

Studies of LPS-CARD interactions may be complicated by the varied acylation and phosphorylation states of this PAMP. In contrast, PGPC offered a precisely defined chemical structure to explore the principles of caspase-11 interactions. Each PGPC molecule is composed of a phosphatidylcholine headgroup, a 16-carbon acyl chain at the first carbon, and a glutaryl group at the second carbon (depicted in fig. S1A). Each of these structural features was examined for its impact on caspase-11 interactions. We first examined the glutaryl group in the interaction with caspase-11, through analysis of 16:0 LysoPC (1-palmitoyl-2-hydroxy-sn-glycero-3-phosphocholine). This lipid shares a comparable structure to PGPC, but lacks the glutaryl group at the second carbon (fig. S1A). Through the limited trypsin digestion assay, we observed that, similar to LPS and PGPC, 16:0 LysoPC

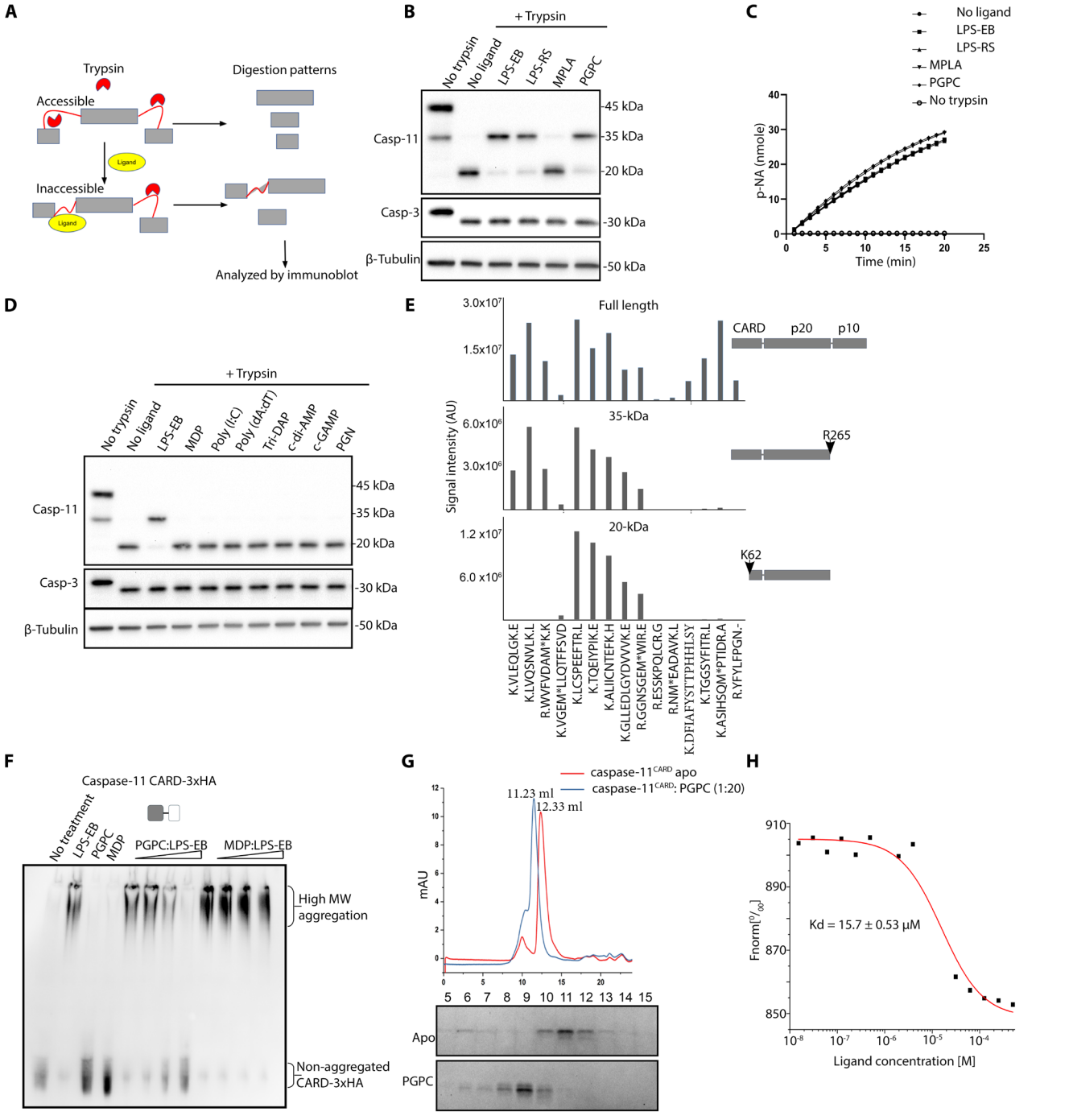

Fig. 2. PGPC binds to the CARD of caspase-11. (**A**) Schematic representation of the principle of limited trypsin digestion. (**B**) 293 T cell lysates containing caspase-11 were treated with various ligands, including LPS from *E. coli* (LPS-EB), *R. sphaeroides* (LPS-RS), monophosphoryl lipid A (MPLA), and PGPC. Lysates were then subjected to limited trypsin digestion followed by immunoblot analysis to detect proteolytic cleavage of caspase-11. (**C**) Trypsin enzymatic activity in the presence of the indicated ligands was measured using a colorimetric assay, quantifying the impact of different ligands on trypsin enzymatic activity. (**D**) Caspase-11–containing cell lysates were treated with various PAMPs, including muramyl dipeptide (MDP), Poly(I), Poly(dA), Tri-DAP (L-Ala-γ-D-Glu-mDAP), c-di-AMP (cyclic di-adenosine monophosphate), cGAMP (cyclic guanosine monophosphate–adenosine monophosphate), and peptidoglycan (PGN). Limited trypsin digestion followed by immunoblotting was performed to assess ligand-induced proteolytic changes in caspase-11. (**E**) Full-length recombinant caspase-11 was incubated with PGPC, subjected to limited trypsin digestion, and analyzed by SDS-PAGE followed by Coomassie staining. Gel bands corresponding to full-length caspase-11 (and cleavage products of 35 and 20 kDa) were further analyzed by mass spectrometry to identify cleavage sites. (**F**) 293T cell lysates expressing HA-tagged caspase-11 CARD with PGPC, LPS-EB, or MDP, alone or in combination, followed by blue native gel electrophoresis and immunoblotting for HA tag. (**G**) Recombinant caspase-11 CARD (amino acids 1 to 80) was incubated with PGPC with the molar ratio 1:20 and subjected to gel filtration chromatography. SDS-PAGE and Coomassie staining were used to analyze eluted fractions. (**H**) Microscale thermophoresis (MST) was performed to determine the binding affinity (K_d) between caspase-11 CARD (amino acids 1 to 80) and PGPC.

protected caspase-11 from digestion, resulting in the 35-kDa protected band on immunoblot (Fig. 3A). The glutaryl group is therefore not necessary to bind caspase-11, indicating that monoacylated lipids can interact with this protein.

To determine the impact of the lipid headgroup on interactions with caspase-11, we performed experiments using a series of 16-carbon monoacylated lipids. These lipids mainly encompassed a diverse range of negatively charged headgroups, spanning from those typically present in membrane phospholipids to the synthetic detergent sodium hexadecyl sulfate (fig. S1A). We found that most of the tested lipids displayed a protective effect on caspase-11 during limited trypsin digestion (Fig. 3A), This finding suggests that caspase-11 can interact with monoacylated lipids containing diverse negatively charged headgroups.

Acyl chain length is the primary determinant of caspase-11 interactions

Given the dispensability of the glutaryl group and the broad tolerance toward various headgroup chemistries, we explored the role of the acyl chain in facilitating caspase-11 interactions. Monoacylated lipids with one or two double bonds exhibited a protective effect on caspase-11 during limited trypsin digestion, suggesting that the degree of saturation in the acyl chain is not a determinant of caspase-11 binding (fig. S1B). We therefore explored the impact of acyl chain length on caspase-11 interactions. Limited trypsin digestion assays were performed in the presence of a spectrum of lysophosphatidylcholines (LysoPCs) that contain acyl chains ranging from 6 carbons (6:0 LysoPC) to 18 carbons (18:0 LysoPC) (fig. S1C). These assays demonstrated that only LysoPCs having acyl chains of 14 carbons or longer protected caspase-11 under limited trypsin digestion (Fig. 3B). Similar results were obtained with lipids having sulfate headgroups, where only lipids comprising a minimum of 12 continuous carbons provided protection against trypsin digestion (fig. S1D). The protective effect of these lipids was also observed in assays using the CARD of caspase-11, akin to our findings with LPS and PGPC (Fig. 3C).

To corroborate these findings, we examined lipid performance in the native PAGE caspase-11 aggregation assays described in Fig. 1. We found that 16:0 LysoPC inhibited the aggregation caspase-11 induced by LPS-EB, whereas 8:0 LysoPC did not (Fig. 3D). The findings suggested acyl chain length discrimination by caspase-11. Consistent with this idea, MST demonstrated that 16:0 LysoPC displayed a binding affinity (K_d) comparable to PGPC (~10 μM). In contrast, 8:0 LysoPC exhibited no detectable interaction with the caspase-11 CARD in this assay (Fig. 3E). Consistent with these findings, 16:0 LysoPC significantly increased the α-helical content of caspase-11, similar to PGPC, while 8:0 LysoPC had minimal impact on caspase-11 secondary structure, as determined by CD spectral analysis (Fig. 3, F and G). These findings indicate that the acyl chain length is a critical determinant governing the capacity of lipids to bind to caspase-11. In particular, lipids containing acyl chains 14 or more carbons in length are the preferred ligand for caspase-11.

Amino acid determinants of caspase-lipid interactions

To determine if acyl chain binding is a conserved feature across mammals, we cloned the CARDs of caspase-11 orthologs (annotated as caspase-4) from various mammalian species and subjected them to limited trypsin digestion. Under the same conditions used for mouse caspase-11, PGPC was found to protect 16 of 22 tested CARDs from tryptic digestion. Notably, this protection was observed even in CARDs that showed no protection when exposed to LPS under the same conditions used to detect LPS and PGPC binding to mouse caspase-11 (Fig. 4A, enlarged version in fig. S2). Acyl chain binding may therefore be a more common feature among mammalian caspase-4 proteins than LPS binding activities. Aligning the sequences that exhibited PGPC protection and comparing them to those that were not protected revealed two conserved phenylalanine residues, Phe^{45} and Phe^{76}, which were abundantly present in the PGPC protected group (fig. S3). Neither of these amino acids have been identified as determinants of caspase-11 function. Although not investigated further herein, we noted that human caspase-5 and the caspases from sheep and lemur do not contain both Phe^{45} and Phe^{76}, but are still protected by PGPC. This finding suggests that other residues may contribute to acyl chain binding.

In silico analysis was used using AlphaFold (*19*) to model the CARD-lipid interaction. This analysis suggested that the CARD has a configuration featuring four amphipathic α-helices, deviating from the conventional six helices found in canonical members of the death domain superfamily (Fig. 4B) (*20*), and is consistent with the reported crystal structure of maltose-binding protein (MBP)–tagged caspase-11 CARD tetramer (*21*). The CARD may also contain a hydrophobic cleft, partly exposed to the solvent (Fig. 4B). To probe the potential of this cleft to accommodate acyl chains, we conducted molecular docking using Swissdock (*22*, *23*). This analysis examined the binding interaction with SDS, which is structurally similar to the smallest sulfate-containing lipid with a 12-carbon chain that protects caspase-11 under limited trypsin digestion (fig. S1D). The docking outcomes revealed a predominant location of SDS within the hydrophobic cleft of the CARD (Fig. 4B). Phe^{76} is positioned within the hydrophobic pocket predicted by AlphaFold (Fig. 4B), suggesting a role in lipid binding. Mutating Phe^{76} to glutamic acid abolished the trypsin protection induced by PGPC and diminished the protective effect of LPS on tryptic digestion (Fig. 4C).

To assess the functional impact of these in vitro findings on caspase-11 activity within cells, we reconstituted caspase-11–deficient immortalized bone marrow–derived macrophages (iBMDMs) with wild type (WT), catalytically inactive (C254A), and acyl chain binding–deficient (F76E) caspase-11 variants. These cells were then subjected to LPS delivery via electroporation. As expected (*17*, *24*), cells expressing WT caspase-11 responded to electroporated LPS by releasing the cytoplasmic proteins interleukin-1β (IL-1β) and lactate dehydrogenase (LDH) into the extracellular space. Also as expected (*17*, *24*), cells expressing the C254A mutant were defective for these LPS responses (Fig. 4D). Consistent with the results from limited trypsin digestion, cells reconstituted with the caspase-11 F76E variant were defective in LPS-induced LDH and IL-1β release at low LPS concentration, with partial responses observed at higher LPS doses. All three cell lines displayed similar LDH release and IL-1β production upon exposure to LPS and nigericin, a stimulus that functions independently of caspase-11 (*24*) (Fig. 4D). Phe^{76}, an amino acid we first identified on the basis of self-ligand (PGPC) interaction studies, is therefore required to bind LPS in vitro and to mediate LPS-induced inflammatory activities within cells.

Two functional regions within the CARD of caspase-11 mediate lipid interactions

While Phe^{76} is required for interactions between caspase-11 and LPS or PGPC, the outcome of these interactions is not identical.

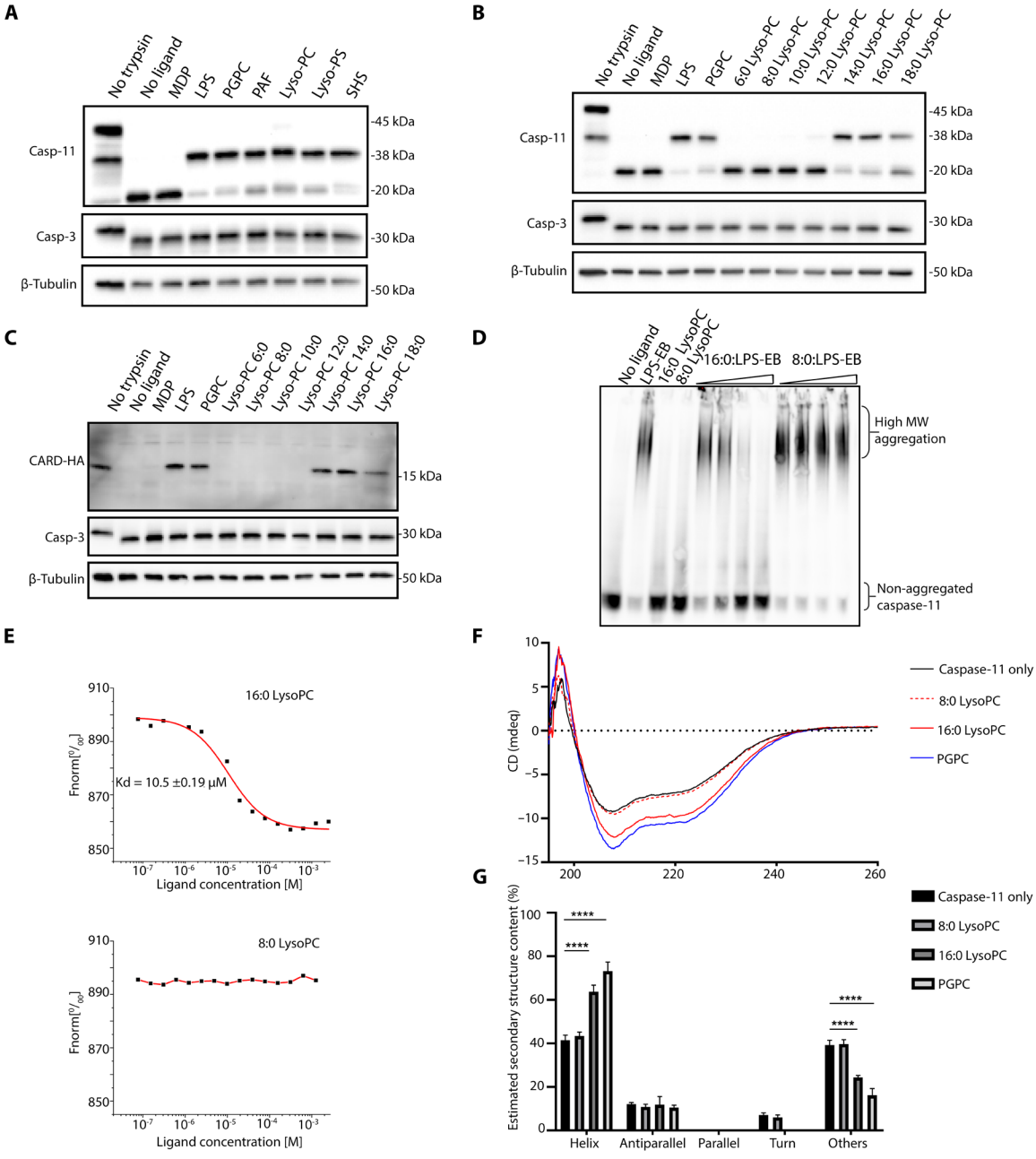

Fig. 3. The binding capacity of lipids to caspase-11 CARD is determined by acyl chain length. (**A**) 293 T cell lysates expressing caspase-11 were treated with various lipids featuring different headgroups, followed by limited trypsin digestion and immunoblotting to assess proteolytic sensitivity. (**B**) Caspase-11–containing cell lysates were treated with lysophosphatidylcholine (LysoPC) with varying acyl chain lengths, subjected to limited trypsin digestion, and analyzed by immunoblotting to detect proteolytic cleavage. (**C**) Lysates containing the caspase-11 CARD domain were treated with lipids of different headgroups, followed by limited trypsin digestion and immunoblot analysis. (**D**) Full-length caspase-11 cell lysates were treated with 16:0 or 8:0 LysoPCs, alone or in combination with LPS-EB, and analyzed by blue native gel electrophoresis followed by immunoblotting to detect caspase-11 aggregation. (**E**) The binding affinity (K_d) between caspase-11 CARD and 16:0 or 8:0 LysoPCs was determined using microscale thermophoresis (MST), highlighting differences in interaction strength between the lipid variants. (**F**) The circular dichroism (CD) spectra of recombinant full-length caspase-11 (0.1 mg/ml) were measured in the absence or presence of various ligands, including PGPC PC (100 μg/ml), 16:0 LysoPC PC (100 μg/ml), and 8:0 Lyso PC (100 μg/ml). (**G**) Quantitative analysis of caspase-11 secondary structure content based on CD spectra deconvolution analyzed by BESTSEL. Data are from three independent experiments, and results with error bars are presented as means ± SEM. Statistical significance was determined by an ordinary two-way ANOVA compared to caspase-11 alone. ns = not significant; *$P < 0.05$, **$P < 0.01$, ***$P < 0.001$, and ****$P < 0.0001$.

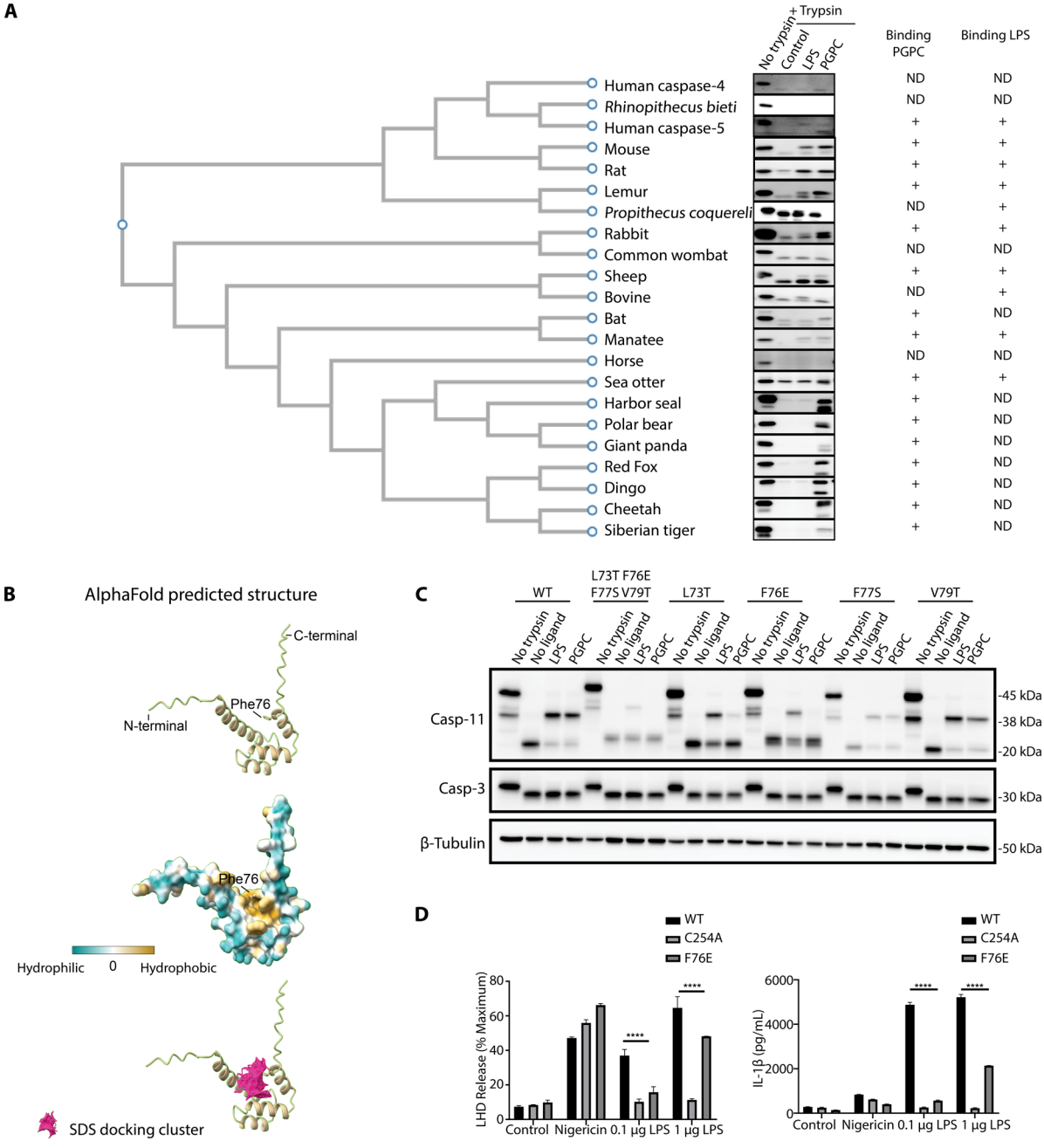

Fig. 4. Structural and functional analysis of caspase-11 CARD homologs and key residue mutants. (**A**) Various mammalian caspase-11 CARD orthologs were exogenously expressed in 293T cells. Cell lysates were incubated with PGPC (100 μg/ml) and LPS (10 μg/ml), followed by limited trypsin digestion. The outcomes were categorized on the basis of a phylogenetic tree constructed using ClustalW. (**B**) AlphaFold-predicted structure of caspase-11 CARD, showing a hypothetical hydrophobic pocket, predicted to accommodate the hydrocarbon chain of SDS by SwissDock. The conserved Phe^{76} is predicted to be at the bottom of the hypothetical hydrophobic pocket. (**C**) Site-directed mutagenesis of hydrophobic residues in the 70 to 80 region of caspase-11 CARD, including the F76E mutation, was expressed in 293T cells. Cell lysates were incubated with PGPC (100 μg/ml) and LPS (10 μg/ml), followed by limited trypsin digestion and immunoblot to detect caspase-11. (**D**) Lactate dehydrogenase (LDH) and IL-1β release in caspase-11 knockout immortalized macrophages reconstituted with caspase-11 variants including the F76E mutation. Cells were electroporated with LPS to assess the functional impact of the CARD variants on cytokine release and cell death. Data are representative of three independent experiments, and results with error bars are presented as means ± SEM. Statistical significance was determined by an ordinary two-way ANOVA compared to AcCARD. ns = not significant; $*P < 0.05$, $**P < 0.01$, $***P < 0.001$, and $****P < 0.0001$.

LPS-induces caspase-11 oligomerization, whereas PGPC does not (Fig. 1). Additional regions within the CARD may therefore mediate the transition from lipid binding to oligomerization. To explore this concept, we examined the N-terminal region of the CARD, upstream of Phe^{45} and Phe^{76}. A series of N-terminal truncated murine caspase-11 mutants was generated and assessed for binding to LPS and PGPC using limited trypsin digestion and native PAGE. The first 10 amino acids proved dispensable for both LPS and PGPC binding. Removal of amino acids 10 to 15 abolished caspase-11 aggregation (Fig. 5A) and LPS binding (Fig. 5B), while the trypsin protective effect induced by PGPC was retained (Fig. 5B). Binding to PGPC was only compromised upon the removal of amino acids 20 to 25 (Fig. 5B). This observation suggests a model in which two functionally distinct regions coexist within the caspase-11 CARD: (i) a C-terminal region responsible for acyl binding, which is independent of aggregation, and (ii) an upstream N-terminal region that also contributes to lipid binding but uniquely facilitates protein aggregation.

If this model is correct, then the two functionally distinct activities within the CARD may be dissociable, and therefore amenable to bioengineering-based manipulation. To test this idea, we sought to engineer CARD-like LPS binding activities within proteins that do not naturally have such functions. Such bioengineering events have been used to rewire the effector domains present in innate immune signal transduction pathway components (*25*, *26*). However, it is unclear if a PRR can be engineered to change ligand specificity. To explore this idea, we first identified additional CARDs that lack LPS binding activity. We used the Foldseek Search Server (*27*), which identifies proteins that share similar tertiary structures and amino acid interactions as those predicted for the caspase-11 CARD by AlphaFold. This in silico analysis identified an uncharacterized CARD-containing protein (UniProt A0A3Q0SFM2) in cichlid fish (*Amphilophus citrinellus*) (hereafter AcCARD) (Fig. 5C). Biochemically, we found that AcCARD binds PGPC in both native PAGE and limited trypsin digestion assays. AcCARD showed no evidence of LPS binding (Fig. 5D). PGPC induced some degree of higher molecular weight AcCARD complexes, by a process that was not inhibited by cotreatment with LPS (Fig. 5D). AcCARD therefore represents a specific PGPC-binding protein, with no ability to bind LPS.

We determined whether we could convert AcCARD into an LPS receptor. Sequence alignment between caspase-11 CARD and AcCARD revealed a relatively conserved sequence in the C terminus. However, the N-terminal residues displayed opposite charges, with positively charged residues in caspase-11 aligning with negatively charged residues in AcCARD. To determine whether the N-terminal region of the caspase-11 CARD could confer LPS-binding activity to AcCARD, we fused the first 38 amino acids of caspase-11 CARD to the PGPC-binding domain of AcCARD (amino acids 39 to 90). This hybrid protein (Casp11-AcCARD) acquired the ability to aggregate and demonstrated protection under limited trypsin digestion in the presence of LPS (Fig. 5E). Furthermore, reconstitution of caspase-11–deficient immortalized macrophages with the hybrid Casp11-AcCARD fused to the catalytic domain of caspase-11 resulted in cell death and IL-1β release in response to LPS electroporation (Fig. 5F). The efficacy of this de novo LPS receptor to induce pyroptosis was further enhanced by incorporating two additional amino acids at position 44 and 45, including the conserved Phe^{45} found in PGPC-protected caspase-4 CARDs (Casp11-AcCARD 44KF45) (Fig. 5, E and F).

Inspection of caspase-11 amino acids 26 to 30 revealed a lysine at position 28, which was absent in the corresponding sequence of AcCARD. Introducing this single substitution into AcCARD (E29K) was sufficient to convert AcCARD into an LPS-binding domain, as demonstrated by both aggregation assays and limited trypsin digestion (Fig. 6A). Furthermore, the LPS-induced aggregation and protective effects were enhanced when an additional mutation at position 20 (D20K), corresponding to the conserved K19 in caspase-11, was introduced (Fig. 6A). Thus, substitution of two amino acids in AcCARD is sufficient to convert this protein from a PGPC receptor into a dual PGPC/LPS receptor, akin to caspase-11. The importance of these amino acids (K19 and K28) in LPS responses by murine caspase-11 was confirmed in reconstituted caspase-11 deficient macrophages. Cells expressing K19 and K28 double mutations were unresponsive to electroporated LPS but retained the ability to respond to LPS + nigericin (Fig. 6B). However, while AcCARD D20K/E29K displayed LPS-binding activity in vitro, cells reconstituted with AcCARD D20K/E29K fused to the caspase-11 catalytic domain failed to respond to electroporated LPS (Fig. 6C). This failure may be attributed to spontaneous autocleavage of the mutant proteins within macrophages, resulting in nonfunctional caspase-11 fragments (Fig. 6D), which warrants further investigation. Nevertheless, the ability to convert a PGPC-binding protein into an LPS receptor in vitro and within cells using chimeric approaches supports the existence of two loosely coupled regions within CARDs. The C-terminal region mediates lipid interactions through hydrophobic interactions, while the upstream N-terminal region uses positively charged residues to link LPS binding to protein aggregation.

Caspase-11 binds to phosphoinositides

Given the role of N-terminal positively charged residues in mediating LPS-binding and aggregation, we reasoned that the corresponding molecular cue in caspase-11 ligands have a negative charge. LPS contains a negatively charged group, in the form of the bis-phosphorylated glucosamine component of lipid A. We reasoned that if lipid headgroup charge was a determinant of caspase-11 interactions, then other phosphorylated lipids should display evidence of caspase-11 interactions. To explore this concept, we examined the interactions between caspase-11 and a variety of eukaryotic lipid species. We used a PIP-strip assay, a method whereby lipids are absorbed onto a hydrophobic membrane and subsequently incubated with recombinant protein (*28*). As this method absorbs hydrophobic acyl chains to the membrane, PIP strip assays selectively report on protein interactions with lipid headgroups. We found that recombinant caspase-11 bound to diverse phosphorylated lipids, including PI(3,4,5)P3 and several phosphatidylinositol bisphosphates (Fig. 6E), which are constituents of eukaryotic cellular membranes (*29*). No detectable interaction was observed with lipids or sphingolipids that lack phosphorylated headgroups (fig. S4). These findings expand the repertoire of self-lipids that caspase-11 can bind beyond PGPC, and suggest preferentially interactions with phosphoinositides with multiple phosphate groups (akin to what is present in bis-phosphorylated LPS). We note caspase-11 did not bind to LysoPC on the PIP strip (fig. S3), despite its ability to protect caspase-11 under limited trypsin digestion (Fig. 3, A to C) and its measured binding affinity (K_d) of 10 μM (Fig. 3E). This finding suggests that LysoPC may interact with caspase-11 primarily through its acyl chains, rather than lipid head groups. This finding supports the general belief that PIP strips report on lipid

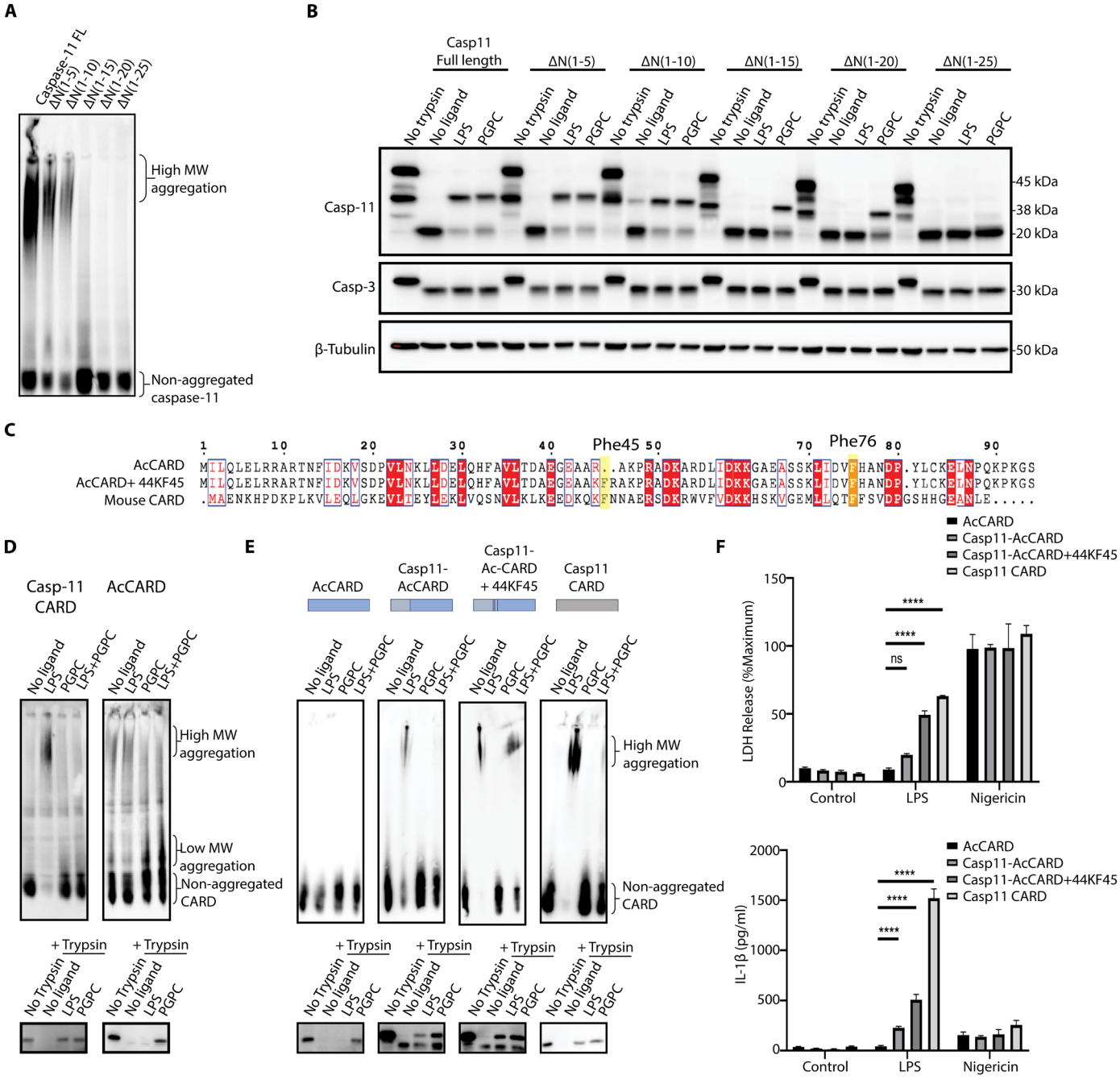

Fig. 5. The N-terminal region of caspase-11 mediates caspase-11 aggregation by LPS. (**A**) 293T cell lysates expressing N-terminal truncated mutants of caspase-11 were incubated with LPS (10 μg/ml). The lysates were analyzed by blue native PAGE followed by immunoblotting to detect caspase-11. (**B**) 293T cell lysates expressing N-terminal truncated mutants of caspase-11 were incubated with LPS (10 μg/ml) and PGPC (100 μg/ml) and subjected to limited trypsin digestion, followed by immunoblotting to detect caspase-11. (**C**) Sequence alignment comparing the CARDs of *A. citrinellus* CARD-containing protein (AcCARD), mouse caspase-11 CARD, and AcCARD with lysine and phenylalanine added at positions 44 and 45 (AcCARD + 44KF45). (**D**) 293T cell lysates expressing HA-tagged AcCARD and caspase-11 CARD were incubated with LPS (10 μg/ml) and PGPC (100 μg/ml) and then subjected to limited trypsin digestion and blue native PAGE followed by immunoblot to detect HA. (**E**) 293T cell lysates expressing engineered HA-tagged AcCARD constructs, where the first 38 amino acids on the N terminus were replaced by the corresponding residues of caspase-11 CARD (Casp11-AcCARD) and an additional variant with K44 and F45 added (Casp11-AcCARD+44KF45), were incubated with LPS (10 μg/ml) and PGPC (100 μg/ml). These lysates were then analyzed by blue native PAGE and limited trypsin digestion, followed by immunoblotting to detect HA. (**F**) IL-1β and LDH release were measured in caspase-11 knockout immortalized macrophages reconstituted with chimeric proteins, where the caspase-11 catalytic domain was fused to different CARD variants. Cells were electroporated with LPS to assess the functional impact of the CARD variants on cytokine release and cell death. Data are representative of two independent experiments, and results with error bars are presented as means ± SEM. Statistical significance was determined by an ordinary one-way ANOVA compared to AcCARD. ns = not significant; **P* < 0.05, ***P* < 0.01, ****P* < 0.001, and *****P* < 0.0001.

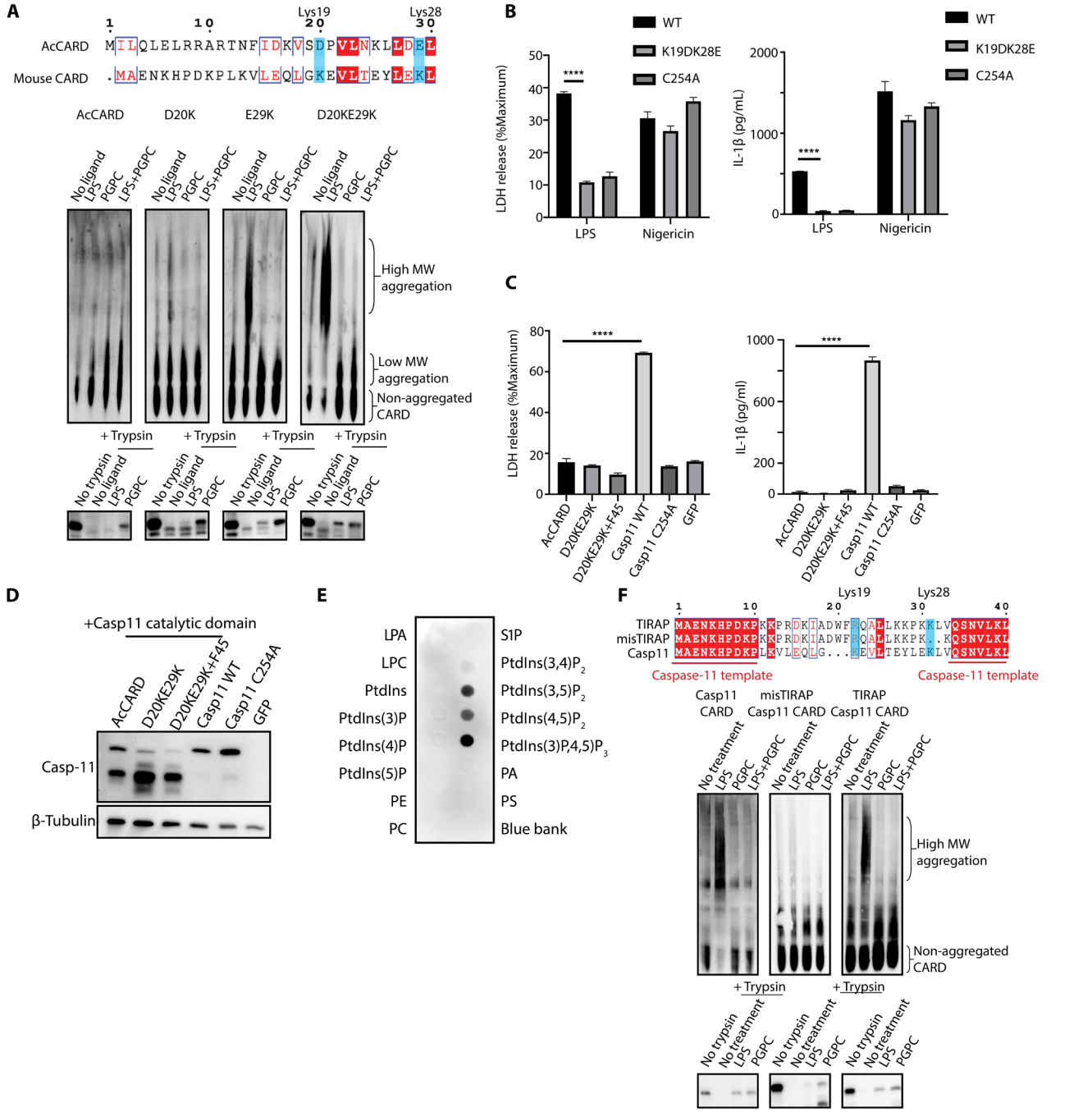

Fig. 6. Caspase-11 binds to phosphoinositides. (**A**) 293T cell lysates expressing HA-tagged AcCARD with mutations converting negatively charged residues to the corresponding positively charged residues in caspase-11 CARD were incubated with LPS (10 μg/ml) and PGPC (100 μg/ml). Lysates were subjected to limited trypsin digestion and blue native PAGE, followed by immunoblotting to detect HA. (**B**) IL-1β and LDH release were measured in caspase-11 knockout immortalized macrophages reconstituted with the K19DK28E mutant and the catalytically inactive mutant C254A. Cells were electroporated with LPS (1 μg per 10^6 cells) to assess the functional impact of these CARD variants on cytokine release and cell death. Data are representative of three independent experiments, and results with error bars are presented as means ± SEM. (**C**) IL-1β and LDH release in caspase-11 knockout immortalized macrophages reconstituted with the caspase-11 catalytic domain fused to AcCARD variants (D20KE29K and D20KE29K + 44KF45), followed by LPS electroporation. Data are representative of three independent experiments, and results with error bars are presented as means ± SEM. (**D**) Immunoblot analysis of caspase-11 fused to different AcCARD variants at the basal state. (**E**) Recombinant caspase-11 was incubated with a PIP-strip containing various phosphoinositides, followed by immunoblot detection to assess phosphoinositide binding by caspase-11. (**F**) 293T cell lysates expressing engineered CARDs containing caspase-11 N-terminal residues (30 to 90) fused to the TIRAP phosphoinositide-binding motif (TIRAP Casp11 CARD) and a misaligned control (misTIRAP Casp11 CARD) were incubated with LPS (10 μg/ml) and PGPC (100 μg/ml). Samples were analyzed by blue native PAGE and limited trypsin digestion, followed by immunoblotting to detect caspase-11 interactions. Statistical significance was determined by an ordinary one-way ANOVA compared to AcCARD. ns = not significant; *$P < 0.05$, **$P < 0.01$, ***$P < 0.001$, and ****$P < 0.0001$.

headgroup interactions, whereas the limited trypsin digestion assay reports on acyl chain interactions.

Proteins interact with phosphoinositide headgroups through electrostatic interactions, whereby positively charged amino acids in a lipid binding domain interact with the negatively charged phosphate groups (*29*). We reasoned that if a similar principle applies to CARD-lipid interactions, then swapping the N-terminal region of caspase-11 with a heterologous phosphoinositide-binding domain should maintain LPS interactions. We therefore engineered a fusion protein between the phosphoinositide-binding domain of TLR adaptor protein TIRAP (*30*) and the C-terminal acyl chain–binding region of caspase-11 CARD. Two chimeric proteins were engineered. One was generated by aligning the positively charged residues in the phosphoinositide-binding domain of TIRAP with the conserved N-terminal positively charged residues in caspase-11 CARD (TIRAP-CARD). A second chimeric protein did not use this alignment to position positively charged residues, referred to herein as misTIRAP-CARD (Fig. 6F). We found that the TIRAP-CARD fusion protein exhibited signatures of LPS-binding, including aggregation and protection under limited trypsin digestion in the presence of LPS (Fig. 6F). In contrast, misTIRAP-CARD, which lacked proper alignment of positively charged residues, did not exhibit evidence of LPS interactions (Fig. 6F). Binding to negative charged headgroups, present on either self (PIPs)– or nonself (LPS)–lipids, is therefore sufficient to link acyl chain binding to aggregation of the CARD of caspase-11.

DISCUSSION

We propose that the caspase-11 ligand is not LPS specifically, but rather any lipid that contains two molecular cues: acyl chains with 14 or more carbons and a negatively charged head group. The N-terminal region of the caspase-11 CARD interacts with the charged lipid headgroup, whereas the C-terminal region mediates acyl chain interactions. Lipids that contain both of these features (e.g., LPS) enable the conversion of caspase-11 from an inactive monomer to an active oligomer that drives pyroptosis and inflammation. Lipids that contain one of these features, such as PGPC monomers, can bind but not aggregate caspase-11 efficiently. While structural analysis will be required to provide unimpeachable evidence to support this model, the strongest functional evidence to support the idea of a bipartite LPS-binding CARD comes from the chimeric proteins we generated. The most notable of these converted a PGPC-binding protein (AcCARD) into an LPS receptor (in vitro and in cells). Further support for this model came from the LPS-binding chimera where the N-terminal caspase-11 region was swapped with the PIP binding domain of TIRAP.

Of the amino acids identified that mediate lipid interactions, K19 was previously shown to be essential for caspase-11 to bind LPS (*17*). While K19 is conserved across all caspase-4 homologs, we identified residue K28, which is uniquely present in rodents (Fig. 4B). This amino acid appears to be a key determinant of aggregation, as K28 is required for LPS-induced aggregation of caspase-11, and introducing K28 into AcCARD was sufficient to confer LPS aggregation. We propose that K28 accounts for the ease at which LPS interactions with caspase-11 can be observed, as compared to other caspases whose LPS binding activity is less easy to detect (e.g., human caspase-4).

Our identification of the essential features of caspase-11 ligands validates the original concept used by Janeway to describe PAMPs (*31*), whereby molecular patterns are detected by PRRs. These patterns can be found in LPS, but also in other (self) lipids. In considering the implications of this finding, it has not escaped our attention that a pivotal question arises. Is self-ligand detection a mistake or a beneficial product of evolution? We consider this question from two perspectives. The first perspective is cell based, and highlights self-ligand detection as a damage-sensing mechanism that may be beneficial for host defense. Hydrophobic moieties, such as acyl chains with 14 or more carbons, are typically absent from the cytosol. These moieties are usually embedded within the hydrophobic regions of membranes or sequestered in lipid droplets, making them inaccessible to cytosolic caspase-11. Therefore, long acyl chains in the cytosol may act as damage-associated molecular patterns detectable by caspase-11, leading to activities that may promote repair and a return to homeostasis. Such activities for caspase-11, if they exist, are undefined.

In addition to freely exposed acyl chains in the cytosol, it is proposed that certain lipid compositions within cellular membranes may disrupt the typical lamellar structure, leading to the exposure of acyl chains that are normally concealed within the bilayer core (*32*). The possibility that acyl chains can be exposed on cellular membranes suggests a context-dependent mechanism for the regulation of caspase-11 binding and activation. Given the requirement for proximity and autoprocessing to achieve full activation (*33*), if these hypotheses hold true, this scenario illustrates a three-dimensional threat-associated molecular pattern, responding to alterations in both the composition and topology of cellular membranes, potentially triggered by pathogen invasion or cellular stress. Furthermore, it is possible that caspase-11 binds phosphoinositides in a physiological context, which would enable interactions with intracellular vesicles, positioning this PRR as a guardian against bacterial escape from phagosomes.

The second perspective on the role of self-ligand detection relates to self-detection as a guardrail to prevent dysfunctional PRR evolution. A key feature of PRRs is their ability to recognize conserved molecular patterns associated with microbial products (i.e., PAMPs). This function must remain stable to ensure their effectiveness in immune defense. However, foreign molecular patterns are not ideal for maintaining consistent selective pressure for three key reasons. First, the same molecular pattern can vary significantly across microbial species, strains, or physiological conditions even for a conserved component like lipid A of LPS (*34*, *35*). Second, threats are rarer and less predictable than nonthreats, with the most successful pathogens often evolving to evade PRRs (*36*). Last, there is significant redundancy in threat detection, with multiple PRRs having the ability to detect individual microbes. This redundancy could enable genetic drift, allowing PRRs to lose their capacity for detection of the original molecular pattern they evolved to detect.

We propose that self-ligands for PRRs may serve as a stable benchmark to preserve the ability of PRRs to recognize molecular patterns effectively. In this regard, it is possible that self-ligand detection by PRRs is not an activity that is counterselected, but rather a fundamental feature that is needed to ensure the biochemical essence of the target ligand remains unchanged throughout evolution. We note that, if this proposed self-first model of PRR function is correct, significant regulatory mechanisms would need to be in place to ensure homeostasis and the induction of inflammation when needed. Such regulatory mechanisms are already evident in the context of nucleic acid–sensing PRRs, as several nucleases and

other enzymes are needed to prevent detection of self-DNA and self-RNA (*12*, *37*–*40*). Whether analogous mechanisms exist for non–nucleic acid–sensing PRRs is presently unclear. The concepts described herein provide a mandate to expand the studies of self-ligand detection to all members of the PRR superfamily.

MATERIALS AND METHODS

Gene cloning

Genes of interest following the Kozak sequence (GCCACC) were cloned into the pMSCV-IRES-GFP (green fluorescent protein) vector between the Xho I and Not I restriction sites. A triple hemagglutinin (HA) tag was added to the C terminus of all CARD structures, linked by a triple glycine-serine (GC) linker (GGGGSGGGGSGGGGSG).

293T transfection

293T cells were seeded 12 to 16 hours before transfection in a six-well plate at a density of 7.5×10^5 cells in a volume of 2 ml per well. On the day of transfection, 2.5 μg of plasmid DNA was diluted in 100 μl of OptiMEM and mixed with 7.5 μl of Lipofectamine in 100 μl of OptiMEM. The Lipofectamine mixture was incubated at room temperature for 15 to 20 min and then combined with the plasmid DNA. The transfection mixture was added dropwise to the wells containing the cells and incubated at 37°C for 16-20 hours.

Cell lysate preparation

On the day following transfection, cell lysates were prepared by adding 200 μl of ice-cold lysis buffer [150 mM NaCl, 25 mM tris (pH 7.5), and 5 mM $MgCl_2$, and 0.05% Triton X-100] to each well. Cells were scraped using a sterile cell scraper, and lysates were vortexed intermittently while incubating on ice for 20 min. Lysates were centrifuged at 16,000*g* for 5 min at 4°C, and the supernatant was collected. Lysates (140 μl, ~600 μg of total protein) were aliquoted into a 96-deep-well plate. To each well, 5 μl of LPS (1 mg/ml; ALX-581-012) or 50 μl of lipids (1 mg/ml) were added, and the total volume was brought to 500 μl with LTD buffer [150 mM NaCl, 25 mM tris (pH 7.5), and 5 mM $MgCl_2$]. The mixture was incubated at room temperature for 30 min.

Limited trypsin digestion

Trypsin (Sigma-Aldrich, T1426) was freshly prepared by weighing 10 mg of trypsin powder and resuspending it in Dulbecco's modified Eagle's medium (DMEM) to a concentration of 1 mg/ml. This was diluted to a 10× concentration of 50 μg/ml with LTD buffer. Fifty microliters of lysate was removed from each well as a time zero control. Fifty microliters of diluted trypsin (50 μg/ml) was added to each well, mixed thoroughly, and incubated. Samples were collected at specific time points, and 50 μl of each sample was added to an equal volume of 2× Laemmli buffer followed by heating at 95°C for 5 min to stop the reaction. For caspase-11 in 293T cell lysates, a 15-min time point was optimal. Samples were then subjected to SDS-PAGE and immunoblot analysis (20 μl per well).

Blue native PAGE

Ten microliters of lysate was incubated with 1 μg of O111:B4 LPS (1 mg/ml; ALX-581-012) and 10 μg of lipids (1 mg/ml; ALX-581-012), with the volume adjusted to 20 μl using ultrapure water. The mixture was incubated at room temperature for 20 min. NativePAGE sample buffer (Thermo Fisher Scientific, BN2003) was then added to the reaction mixture. The samples were loaded onto NativePAGE 4 to 16% (Thermo Fisher Scientific, BN1004BOX) Bis-Tris Protein Gels (1.0 mm, 15-well) and run according to the protocol for immunoblot analysis, using dark blue buffer (Thermo Fisher Scientific, BN2002) for the first third of the gel and light blue buffer for the remainder. The gel was subsequently transferred to a polyvinylidene difluoride (PVDF) membrane for immunoblot analysis.

Competitive binding assay

Ten microliters of lysate were incubated with 1 μg of O111:B4 LPS (1 mg/ml; Enzo ALX-581-012) and increasing concentrations of LPS-RS (0.5, 1, 5, and 10 w/w), PGPC (1.25, 2.5, 5, and 10 w/w), and MDP (1.25, 2.5, 5, and 10 w/w) for 20 min at room temperature, followed by blue native PAGE analysis.

Recombinant protein production and purification

pFastBac plasmid encoding full-length caspase-11 with a C254A mutation and N-terminal His tag was a gift from J. Ruan (University of Connecticut), and the protein was produced in Sf9 insect cells. Chemically competent DH10Bac cells (Thermo Fisher Scientific) were transformed with the pFastBac vector encoding caspase-11 C254A and plated on LB agar plates containing kanamycin (25 μg/ml), tetracycline (10 μg/ml), gentamycin (7 μg/ml), X-Gal (50 μg/ml), and isopropyl-β-D-thiogalactopyranoside (40 μg/ml), and incubated overnight at 37°C for blue/white screening. A single white colony was inoculated into 20 ml of LB medium with kanamycin (25 μg/ml), tetracycline (10 μg/ml), and gentamycin (7 μg/ml) and incubated overnight at 37°C and 250 rpm. Bacmid DNA was isolated using buffer components from the GeneJET Plasmid Miniprep kit (Thermo Fisher Scientific) and precipitated using isopropanol. The DNA pellet was washed once with 70% ethanol, air dried, and resuspended in 40 μl of sterile, ultrapure water. Ten microliters of bacmid DNA-containing water was diluted with 100 μl of Hyclone SFX insect cell media. Ten microliters of CellFectin II (Thermo Fisher Scientific) transfection reagent was mixed with 100 μl of media and added to the DNA mixture. After incubating at room temperature for 30 min, 100 μl of the transfection mix was added dropwise to 0.8×10^6 Sf9 cells seeded in a six-well plate with 3 ml of media. After 2 to 3 days of incubation at 28°C, the baculovirus-containing supernatant was collected. Virus-containing supernatants from two wells were combined, filtered using a 0.45-μm syringe filter, and stored at 4°C. To amplify the virus, Sf9 cells were grown to a density of 1.0×10^6 cells/ml in 25 ml, infected with 2 ml of the initial virus, and incubated at 28°C and 120 rpm. After 3 days, virus was collected by centrifuging the cells at 1000*g* for 10 min, and the supernatant was filtered (0.45-μm syringe filter) and stored at 4°C. For protein expression, Sf9 cells were seeded at a density of 1.5×10^6 cells/ml in a 1-liter suspension culture, infected with 1% (v/v) of the amplified virus, and incubated at 28°C and 120 rpm. After 96 hours of incubation, cell proliferation arrested and cells were harvested by centrifugation at 1000*g* for 15 min. Cell pellets were frozen in liquid nitrogen and stored at −20°C until protein purification. For protein purification, frozen cell pellets were resuspended in 100 ml of resuspension buffer [25 mM HEPES-NaOH (pH 7.4), 150 mM NaCl, and 10 mM imidazole] and lysed by ultrasonication. The lysate was clarified by centrifugation at 20,000*g* for 45 min at 4°C. The supernatant was incubated with 1 ml of Ni–nitrilotriacetic acid agarose beads (Qiagen) pre-equilibrated in resuspension buffer for 1 hour at 4°C with gentle rotation. The beads were collected by centrifugation,

resuspended in 10 ml of resuspension buffer, and transferred to a gravity flow column. The beads were washed with 20 bed volumes of wash buffer [25 mM HEPES-NaOH (pH 7.4), 400 mM NaCl, and 25 mM imidazole], and bound protein was eluted in 10 ml of elution buffer [25 mM HEPES-NaOH (pH 7.4), 150 mM NaCl, and 250 mM imidazole]. Eluted protein was concentrated using Amicon Ultra-15 centrifugal filter units with a 10-kDa cutoff (EMD Millipore) and further purified by size exclusion chromatography using a BioRad NGC Quest10 Chromatography system equipped with a Superdex 200 Increase 10/300 column in SEC buffer [25 mM HEPES-NaOH (pH 7.4) and 150 mM NaCl]. Fractions containing pure caspase-11 were identified by SDS-PAGE and InstantBlue staining (Expedeon) and combined. Glycerol was added to the combined fractions to a final concentration of 10%. Protein concentration was measured by absorbance at 280 nm using a Nanodrop device, corrected for the protein-specific extinction coefficient. Aliquots with a protein concentration between 0.5 and 1 mg/ml were snap-frozen in liquid nitrogen and stored at −80°C.

Bioinformatic analysis

Predicting structure using AlphaFold, the first 90 amino acids were defined as the CARD of caspase-11. The amino acid sequence was input into the AlphaFold Colab Page (version 1.5.2) using MMseqs2 in unpaired mode. Models were ranked on the basis of the predicted local distance difference test (plddt) scores, with autoselection for the model type and the number of recycles. The PDB file of the top-ranked model was selected as the predicted structure for caspase-11 CARD. The predicted structure of caspase-11 CARD was used as the target for ligand docking in SwissDock (old version: old.swissdock.ch/docking). SDS (ZINC1532179) was selected as the ligand. Orthologs searching using Foldseek (https://search.foldseek.com/search): The predicted structure of caspase-11 CARD was used as the input for Foldseek server to search on AlphaFold/UniProt50, CATH50, and PDB100. The returned structures were examined manually. Candidates were cloned to pMSCV-IRES-GFP backbone. Sequence alignment was performed using CLUSTALW (www.genome.jp/tools-bin/clustalw), illustrated using ESPript3 (https://espript.ibcp.fr/ESPript/ESPript/).

Limited trypsin digestion with recombinant protein and mass spectrometry

Two micrograms of recombinant full-length catalytically inactive caspase-11 C254A was reconstituted in 10 μl of LTD buffer and incubated with 10 μg of PGPC (1 mg/ml) at room temperature for 20 min. Five microliters of freshly prepared trypsin (50 μg/ml) was added to each reaction, followed by incubation. The reaction was stopped by adding 2× Laemmli buffer after 2 min and heating at 95°C for 5 min. Fifteen microliters of each sample was loaded onto NuPAGE Bis-Tris Mini Protein Gels, 4 to 12% (1.0 mm, NP0321BOX) and electrophoresed. Corresponding protein bands were visualized using InstantBlue Coomassie Protein Stain (Abcam, ISB1L) and rinsed with distilled water. The corresponding gel bands were excised and sent for liquid chromatography–tandem mass spectrometry (LC-MS/MS).

Protein sequence analysis by LC-MS/MS

Excised gel bands were cut into approximately 1-mm^3 pieces. Gel pieces were then subjected to a modified in-gel trypsin digestion procedure. Gel pieces were washed and dehydrated with acetonitrile for 10 min. Followed by removal of acetonitrile. Pieces were then completely dried in a speed-vac. Rehydration of the gel pieces was with 50 mM ammonium bicarbonate solution containing modified sequencing-grade trypsin (12.5 ng/μl; Promega, Madison, WI) at 4°C. After 45 min, the excess trypsin solution was removed and replaced with 50 mM ammonium bicarbonate solution to just cover the gel pieces. Samples were then placed in a 37°C room overnight. Peptides were later extracted by removing the ammonium bicarbonate solution, followed by one wash with a solution containing 50% acetonitrile and 1% formic acid. The extracts were then dried in a speed-vac (~1 hour). The samples were then stored at 4°C until analysis. On the day of analysis, the samples were reconstituted in 5 to 10 μl of high-performance LC (HPLC) solvent A (2.5% acetonitrile and 0.1% formic acid). A nanoscale reverse-phase HPLC capillary column was created by packing 2.6-μm C18 spherical silica beads into a fused silica capillary (100 μm inner diameter × ~30 cm length) with a flame-drawn tip. After equilibrating the column each sample was loaded via a Famos autosampler (LC Packings, San Francisco CA) onto the column. A gradient was formed and peptides were eluted with increasing concentrations of solvent B (97.5% acetonitrile and 0.1% formic acid). As peptides eluted, they were subjected to electrospray ionization and then entered into a Velos Orbitrap Pro ion-trap mass spectrometer (Thermo Fisher Scientific, Waltham, MA). Peptides were detected, isolated, and fragmented to produce a tandem mass spectrum of specific fragment ions for each peptide. Peptide sequences (and hence protein identity) were determined by matching protein databases with the acquired fragmentation pattern by the software program, Sequest (Thermo Fisher Scientific, Waltham, MA). All databases include a reversed version of all the sequences and the data was filtered to between a one and 2% peptide false discovery rate.

CD spectroscopy

CD spectra were recorded using a Jasco J-1500 CD spectropolarimeter equipped with a Peltier temperature controller. Recombinant full-length caspase-11 protein was prepared in a buffer containing 150 mM NaCl, 5 mM $MgCl_2$, and 25 mM tris (pH 7.4) at a concentration of 0.1 mg/ml. Ligands, including MDP, LPS-EB, LPS-RS, PGPC, 16:0 LysoPC, and 8:0 LysoPC, were added at a concentration of 100 μg/ml before measurement. The samples were loaded into a 1-mm pathlength quartz cuvette, and spectra were collected at 20°C. Wavelength scans were performed from 195 to 260 nm with a 1 nm increment. A total of five scans were averaged for each sample. Buffer baselines were collected under identical conditions and subtracted from the protein-ligand spectra. Secondary structure content was estimated by deconvoluting the CD spectra using BESTSEL platform. All measurements were performed at least in triplicate, and data are presented as mean ± SD.

Recombinant CARD and liquid chromatography

pFastBac plasmid encoding caspase-11 CARD domain was expressed and purified similarly to full-length caspase-11 with a C254A mutation. The purified caspase-11 CARD was further purified with size exclusion chromatography [Superdex 200 (10/300)] with buffer A (150 mM NaCl and 25 mM tris-HCl, pH8.0). Fractions containing pure caspase-11 were identified by SDS-PAGE. Pure protein (final concentration, 20 μM) was mixed with PGPC (final concentration, 400 μM) at a 1:20 molar ratio in a total volume of 500 μl and incubated for 10 min. The mixture was then sonicated for 1 min

(10% power, 1 s on, and 3 s off). Then, the sample centrifuged for 30 min, 1400 rpm. The sample finally was loaded on the Superdex75 (10/300) with buffer A (150 mM NaCl and 25 mM tris-HCl, pH8.0). Caspase-11 CARD alone sample without PGPC was done with all the processing steps at the same time.

Microscale thermophoresis

Plasmid encoding MBP-tagged caspase-11 CARD protein containing an extra cysteine amino acid was used for caspase-11 CARD expression and purification. The purified protein from gel filtration was mixed with Alexa Fluor 647 C2 Maleimide (Invitrogen, A20347) at the molar ratio of 1:2, with the tube covered with aluminium foil paper to avoid light. Incubation of the mixture proceeded at 4°C overnight. The mixture was added to a Superdex 200 (10/300) with buffer B [25 mM HEPES (pH7.5) and 150 mM NaCl] to obtain pure labeled caspase-11 CARD protein for MST assay. MST experiments were performed according to the manufacturer's instructions (NanoTemper Technologies, Monolith). The protein concentration applied in the assay was 50 nM and the ligand was started at highest concentration of 500 μM. A serial dilution of the ligand was applied in the assay. After incubation of protein and ligands, samples were loaded filled into MST Premium coated capillaries (NanoTemper Technologies monolith, act no. MO-K025) and measurements were taken at a constant temperature of 16°C. The MO.Affinity Analysis Software (NanoTemper) was used to analyze the binding affinity and the K_d value (dissociation constant) with the fitting model. The thermophoretic movement changes were represented by the normalized fluorescence ratio difference before and after heating (ΔFnorm [‰]) and plotted against ligand concentration. The binding curve generated was then fitted using software to determine binding constants and calculate the dissociation constant (K_d).

Cell culture, retroviral transduction, and selection of caspase-11$^{-/-}$ macrophages

Caspase-11$^{-/-}$ iBMDMs were cultured in DMEM supplemented with 10% fetal bovine serum (FBS), penicillin-streptomycin, L-glutamine, and sodium pyruvate. 293T cells were used as a packaging cell line for retroviral vectors. For the production of retroviral particles, 7.5×10^5 293T cells were seeded in each well of six-well plate. After overnight incubation at 37°C, the cells were transfected with 1.5 μg of pMSCV IRES enhanced GFP encoding the protein of interest, 1 μg of pCL-ECO, and 0.5 μg of pCMV-VSVG using 9-μl Lipofectamine 2000 in 150 μl total volume (Thermo Fisher Scientific) according to the manufacturer's instructions. After 16 hours at 37°C, the media were replaced with 2 ml of fresh complete media with additional FBS (30% in final concentration). The virus-containing supernatant was collected 24 hours after the media change. Supernatants were clarified by centrifugation at 400*g* for 5 min and filtered through a 0.45-μm PVDF syringe filter. Approximately 1×10^5 caspase-11$^{-/-}$ iBMDMs were transduced twice on consecutive days in a 12-well plate by adding 1.5 ml of viral supernatant, supplemented with polybrene (1:2000; EMD Millipore) per well. The plates were centrifuged at 1250*g* for 1 hour at 30°C. After centrifuge, 1.0 ml of fresh media was added to each well. Cells were subjected to the second round of centrifugation with virus-containing supernatant after 24 hours. Cells were transferred to fresh media after 24 hours and were allowed to expand to be sorted twice using FACSMelody cell sorter (BD Biosciences) to generate cell lines with stable and homogeneous expression of the target gene. Transgene expression was confirmed by immunoblotting using a rat anti–caspase-11 antibody (Cell Signaling Technologies, 14340).

Cytoplasmic delivery of bacterial LPS using the Neon Transfection System

Murine iBMDMs were transfected with bacterial LPS using the Neon Transfection System (Thermo Fisher Scientific). Cells were first primed with R848 for 3 hours, then lifted with PBS + EDTA and resuspended in R buffer at a concentration of 10×10^6 cells/ml. The cell suspension was mixed with either LPS (1 μg per 1×10^6 cells) or sterile PBS (1 μl per 1×10^6 cells as a control). The mixture was aspirated into a 100-μl electroporation pipette tip, and electroporation was performed with two pulses, each 10 ms long, at 1400 V (unless otherwise specified). The transfected cells were transferred into media at 1×10^6 cells/ml and seeded into 96-well plates at 100 μl per well. For the nigericin-treated control, lifted iBMDM was added directly to nigericin containing media (10 μM) at the same cell concentration as the LPS electroporated cells. Cell death and IL-1β release were measured 6 hours later using an LDH assay and a Lumit assay, respectively.

Cell death assays, IL-1β release, and trypsin activity quantification

Cell lysis was assessed using the CyQuant LDH Cytotoxicity Assay Kit (Thermo Fisher Scientific). Twenty-five microliters of supernatant was mixed with 25 μl of LDH assay buffer and incubated at room temperature for 15 min. Absorbance was measured at 490 and 680 nm using a Tecan Spark plate reader, and the signal was normalized to the lysis controls. IL-1β levels were quantified using the Promega Lumit Mouse IL-1β Immunoassay. Twenty-five microliters of sample were mixed with 25 μl of antibody mixture and incubated at 37°C for 1 hour. A total of 12.5 μl of luminescence substrate was added, and the luminescent signal was measured using a Tecan Spark plate reader. Trypsin activity was measured using trypsin activity assay kit (ab102531).

Statistical analysis

Statistical significance was assessed using one-way analysis of variance (ANOVA) followed by Tukey's multiple comparison test. A P value of less than 0.05 was considered statistically significant. All statistical analyses were performed using GraphPad Prism data analysis software. Data are representative of at least two independent experiments, and results with error bars are presented as means ± SEM.

Supplementary Materials

This PDF file includes:

Figs. S1 to S4

REFERENCES AND NOTES

1. U. Koch, F. Radtke, Mechanisms of T cell development and transformation. *Annu. Rev. Cell Dev. Biol.* **27**, 539–562 (2011).
2. L. Klein, B. Kyewski, P. M. Allen, K. A. Hogquist, Positive and negative selection of the T cell repertoire: What thymocytes see (and don't see). *Nat. Rev. Immunol.* **14**, 377–391 (2014).
3. R. Medzhitov, Approaching the asymptote: 20 years later. *Immunity* **30**, 766–775 (2009).
4. G. Liu, H. Zhang, C. Zhao, H. Zhang, Evolutionary history of the toll-like receptor gene family across vertebrates. *Genome Biol. Evol.* **12**, 3615–3634 (2020).
5. B. M. P. Ngou, M. Wyler, M. W. Schmid, Y. Kadota, K. Shirasu, Evolutionary trajectory of pattern recognition receptors in plants. *Nat. Commun.* **15**, 308 (2024).

6. L. Z. Kong, S. M. Kim, C. Wang, S. Y. Lee, S. C. Oh, S. Lee, S. Jo, T. D. Kim, Understanding nucleic acid sensing and its therapeutic applications. *Exp. Mol. Med.* **55**, 2320–2331 (2023).
7. M. Motwani, S. Pesiridis, K. A. Fitzgerald, DNA sensing by the cGAS–STING pathway in health and disease. *Nat. Rev. Genet.* **20**, 657–674 (2019).
8. M. Schlee, G. Hartmann, Discriminating self from non-self in nucleic acid sensing. *Nat. Rev. Immunol.* **16**, 566–580 (2016).
9. B. Hu, C. Jin, H. B. Li, J. Tong, X. Ouyang, N. M. Cetinbas, S. Zhu, T. Strowig, F. C. Lam, C. Zhao, J. Henao-Mejia, O. Yilmaz, K. A. Fitzgerald, S. C. Eisenbarth, E. Elinav, R. A. Flavell, The DNA-sensing AIM2 inflammasome controls radiation-induced cell death and tissue injury. *Science* **354**, 765–768 (2016).
10. L. S. Huang, Z. Hong, W. Wu, S. Xiong, M. Zhong, X. Gao, J. Rehman, A. B. Malik, mtDNA Activates cGAS signaling and suppresses the YAP-mediated endothelial cell proliferation program to promote inflammatory injury. *Immunity* **52**, 475–486.e5 (2020).
11. V. A. K. Rathinam, Z. Jiang, S. N. Waggoner, S. Sharma, L. E. Cole, L. Waggoner, S. K. Vanaja, B. G. Monks, S. Ganesan, E. Latz, V. Hornung, S. N. Vogel, E. Szomolanyi-Tsuda, K. A. Fitzgerald, The AIM2 inflammasome is essential for host defense against cytosolic bacteria and DNA viruses. *Nat. Immunol.* **11**, 395–402 (2010).
12. C. Uggenti, A. Lepelley, Y. J. Crow, Self-awareness: Nucleic acid–driven inflammation and the type I interferonopathies. *Annu. Rev. Immunol.* **37**, 247–267 (2019).
13. L. H. Chu, M. Indramohan, R. A. Ratsimandresey, A. Gangopadhyay, E. P. Morris, D. M. Monack, A. Dorfleutner, C. Stehlik, The oxidized phospholipid oxPAPC protects from septic shock by targeting the non-canonical inflammasome in macrophages. *Nat. Commun.* **9**, 996 (2018).
14. C. Erridge, S. Kennedy, C. M. Spickett, D. J. Webb, Oxidized phospholipid inhibition of Toll-like receptor (TLR) signaling is restricted to TLR2 and TLR4: Roles for CD14, LPS-binding protein, and MD2 as targets for specificity of inhibition. *J. Biol. Chem.* **283**, 24748–24759 (2008).
15. I. Zanoni, Y. Tan, M. D. Gioia, A. Broggi, J. Ruan, J. Shi, C. A. Donado, F. Shao, H. Wu, J. R. Springstead, J. C. Kagan, An endogenous caspase-11 ligand elicits interleukin-1 release from living dendritic cells. *Science* **352**, 1232–1236 (2016).
16. I. Zanoni, Y. Tan, M. D. Gioia, J. R. Springstead, J. C. Kagan, By capturing inflammatory lipids released from dying cells, the receptor CD14 induces inflammasome-dependent phagocyte hyperactivation. *Immunity* **47**, 697–709.e3 (2017).
17. J. Shi, Y. Zhao, Y. Wang, W. Gao, J. Ding, P. Li, L. Hu, F. Shao, Inflammatory caspases are innate immune receptors for intracellular LPS. *Nature* **514**, 187–192 (2014).
18. A. H. Pande, S. Kar, R. K. Tripathy, Oxidatively modified fatty acyl chain determines physicochemical properties of aggregates of oxidized phospholipids. *Biochim. Biophys. Acta* **1798**, 442–452 (2010).
19. M. Mirdita, K. Schütze, Y. Moriwaki, L. Heo, S. Ovchinnikov, M. Steinegger, ColabFold: Making protein folding accessible to all. *Nat. Methods* **19**, 679–682 (2022).
20. H. H. Park, Y. C. Lo, S. C. Lin, L. Wang, J. K. Yang, H. Wu, The death domain superfamily in intracellular signaling of apoptosis and inflammation. *Annu. Rev. Immunol.* **25**, 561–586 (2007).
21. M. Liu, K. Zhou, Z. Xu, H. Ma, X. Cao, X. Yin, W. Zeng, A. Zahid, S. Fu, K. Ni, X. Ye, Y. Zhou, L. Bai, R. Zhou, T. Jin, Crystal structure of caspase-11 CARD provides insights into caspase-11 activation. *Cell Discov.* **6**, 70 (2020).
22. A. Grosdidier, V. Zoete, O. Michielin, SwissDock, a protein-small molecule docking web service based on EADock DSS. *Nucleic Acids Res.* **39**, W270–W277 (2011).
23. A. Grosdidier, V. Zoete, O. Michielin, Fast docking using the CHARMM force field with EADock DSS. *J. Comput. Chem.* **32**, 2149–2159 (2011).
24. N. Kayagaki, S. Warming, M. Lamkanfi, L. V. Walle, S. Louie, J. Dong, K. Newton, Y. Qu, J. Liu, S. Heldens, J. Zhang, W. P. Lee, M. Roose-Girma, V. M. Dixit, Non-canonical inflammasome activation targets caspase-11. *Nature* **479**, 117–121 (2011).
25. P. Devant, A. Cao, J. C. Kagan, Evolution-inspired redesign of the LPS receptor caspase-4 into an interleukin-1β–converting enzyme. *Sci. Immunol.* **6**, eabh3567 (2021).
26. Y. Tan, J. C. Kagan, Innate immune signaling organelles display natural and programmable signaling flexibility. *Cell* **177**, 384–398.e11 (2019).
27. M. van Kempen, S. S. Kim, C. Tumescheit, M. Mirdita, J. Lee, C. L. M. Gilchrist, J. Söding, M. Steinegger, Fast and accurate protein structure search with Foldseek. *Nat. Biotechnol.* **42**, 243–246 (2024).
28. C. M. Shirey, J. L. Scott, R. V. Stahelin, Notes and tips for improving quality of lipid-protein overlay assays. *Anal. Biochem.* **516**, 9–12 (2017).
29. Y. Posor, W. Jang, V. Haucke, Phosphoinositides as membrane organizers. *Nat. Rev. Mol. Cell Biol.* **23**, 797–816 (2022).
30. J. C. Kagan, R. Medzhitov, Phosphoinositide-mediated adaptor recruitment controls Toll-like receptor signaling. *Cell* **125**, 943–955 (2006).
31. C. A. Janeway Jr., Approaching the asymptote? Evolution and revolution in immunology. *Cold Spring Harb. Symp. Quant. Biol.* **54**, 1–13 (1989).
32. F. Scollo, C. Tempra, H. Evci, M. Riopedre-Fernandez, A. Olżyńska, M. Javanainen, A. Uday, M. Cebecauer, L. Cwiklik, H. Martinez-Seara, P. Jungwirth, P. Jurkiewicz, M. Hof, Can calmodulin bind to lipids of the cytosolic leaflet of plasma membranes? *Open Biol.* **14**, 240067 (2024).
33. C. Ross, A. H. Chan, J. V. Pein, D. Boucher, K. Schroder, Dimerization and auto-processing induce caspase-11 protease activation within the non-canonical inflammasome. *Life Sci. Alliance* **6**, e201800237 (2018).
34. F. Dardelle, C. Phelip, M. Darabi, T. Kondakova, X. Warnet, E. Combret, E. Juranville, A. Novikov, J. Kerzerho, M. Caroff, Diversity, complexity, and specificity of bacterial lipopolysaccharide (LPS) structures impacting their detection and quantification. *Int. J. Mol. Sci.* **25**, 3927 (2024).
35. R. F. Maldonado, I. Sá-Correia, M. A. Valvano, Lipopolysaccharide modification in Gram-negative bacteria during chronic infection. *FEMS Microbiol. Rev.* **40**, 480–493 (2016).
36. J. C. Kagan, Infection infidelities drive innate immunity. *Science* **379**, 333–335 (2023).
37. Y. J. Crow, D. S. Chase, J. Lowenstein Schmidt, M. Szynkiewicz, G. M. A. Forte, H. L. Gornall, A. Oojageer, B. Anderson, A. Pizzino, G. Helman, M. S. Abdel-Hamid, G. M. Abdel-Salam, S. Ackroyd, A. Aeby, G. Agosta, C. Albin, S. Allon-Shalev, M. Arellano, G. Ariaudo, V. Aswani, R. Babul-Hirji, E. M. Baildam, N. Bahi-Buisson, K. M. Bailey, C. Barnerias, M. Barth, R. Battini, M. W. Beresford, G. Bernard, M. Bianchi, T. Billette de Villemeur, E. M. Blair, M. Bloom, A. B. Burlina, M. Luisa Carpanelli, D. R. Carvalho, M. Castro-Gago, A. Cavallini, C. Cereda, K. E. Chandler, D. A. Chitayat, A. E. Collins, C. Sierra Corcoles, N. J. V. Cordeiro, G. Crichiutti, L. Dabydeen, R. C. Dale, S. D'Arrigo, C. G. E. L. de Goede, C. de Laet, L. M. H. de Waele, I. Denzler, I. Desguerre, K. Devriendt, M. di Rocco, M. C. Fahey, E. Fazzi, C. D. Ferrie, A. Figueiredo, B. Gener, C. Goizet, N. R. Gowrinathan, K. Gowrishankar, D. Hanrahan, B. Isidor, B. Kara, N. Khan, M. D. King, E. P. Kirk, R. Kumar, L. Lagae, P. Landrieu, H. Lauffer, V. Laugel, R. L. Piana, M. J. Lim, J. P. S. M. Lin, T. Linnankivi, M. T. Mackay, D. R. Marom, C. Marques Lourenço, S. A. McKee, I. Moroni, J. E. V. Morton, M. L. Moutard, K. Murray, R. Nabbout, S. Nampoothiri, N. Nunez-Enamorado, P. J. Oades, I. Olivieri, J. R. Ostergaard, B. Pérez-Dueñas, J. S. Prendiville, V. Ramesh, M. Rasmussen, L. Régal, F. Ricci, M. Rio, D. Rodriguez, A. Roubertie, E. Salvatici, K. A. Segers, G. P. Sinha, D. Soler, R. Spiegel, T. I. Stödberg, R. Straussberg, K. J. Swoboda, M. Suri, U. Tacke, T. Y. Tan, J. te Water Naude, K. Wee Teik, M. Mary Thomas, M. Till, D. Tonduti, E. Maria Valente, R. Noel van Coster, M. S. van der Knaap, G. Vassallo, R. Vijzelaar, J. Vogt, G. B. Wallace, E. Wassmer, H. J. Webb, W. P. Whitehouse, R. N. Whitney, M. S. Zaki, S. M. Zuberi, J. H. Livingston, F. Rozenberg, P. Lebon, A. Vanderver, S. Orcesi, G. I. Rice, Characterization of human disease phenotypes associated with mutations in TREX1, RNASEH2A, RNASEH2B, RNASEH2C, SAMHD1, ADAR, and IFIH1. *Am. J. Med. Genet. A* **167**, 296–312 (2015).
38. S. Jimeno, R. Prados-Carvajal, M. J. Fernández-Ávila, S. Silva, D. A. Silvestris, M. Endara-Coll, G. Rodríguez-Real, J. Domingo-Prim, F. Mejías-Navarro, A. Romero-Franco, S. Jimeno-González, S. Barroso, V. Cesarini, A. Aguilera, A. Gallo, N. Visa, P. Huertas, ADAR-mediated RNA editing of DNA:RNA hybrids is required for DNA double strand break repair. *Nat. Commun.* **12**, 5512 (2021).
39. M. P. Rodero, A. Tesser, E. Bartok, G. I. Rice, E. Della Mina, M. Depp, B. Beitz, V. Bondet, N. Cagnard, D. Duffy, M. Dussiot, M. L. Frémond, M. Gattorno, F. Guillem, N. Kitabayashi, F. Porcheray, F. Rieux-Laucat, L. Seabra, C. Uggenti, S. Volpi, L. A. H. Zeef, M. A. Alyanakian, J. Beltrand, A. M. Bianco, N. Boddaert, C. Brouzes, S. Candon, R. Caorsi, M. Charbit, M. Fabre, F. Faletra, M. Girard, A. Harroche, E. Hartmann, D. Lasne, A. Marcuzzi, B. Neven, P. Nitschke, T. Pascreau, S. Pastore, C. Picard, P. Picco, E. Piscianz, M. Polak, P. Quartier, M. Rabant, G. Stocco, A. Taddio, F. Uettwiller, E. Valencic, D. Vozzi, G. Hartmann, W. Barchet, O. Hermine, B. Bader-Meunier, A. Tommasini, Y. J. Crow, Type I interferon-mediated autoinflammation due to DNase II deficiency. *Nat. Commun.* **8**, 2176 (2017).
40. D. B. Stetson, J. S. Ko, T. Heidmann, R. Medzhitov, Trex1 prevents cell-intrinsic initiation of autoimmunity. *Cell* **134**, 587–598 (2008).

Acknowledgments: We thank members of the Kagan lab for helpful discussions. **Funding:** This study was supported by NIH grants AI167993, AI116550, and DK34854 to J.C.K. and AI158435 to J.R. **Author contributions:** Conceptualization: J.C.K. and A.B.C. Methodology: W.M., P.D., C.W., and A.B.C. Investigation: A.B.C. and C.W. Visualization: A.B.C. and C.W. Validation: M.S. Supervision: J.C.K. and J.R. Writing–original draft: J.C.K. and A.B.C. Writing–review and editing: J.C.K., A.B.C., S.N.K., and M.S. Resources: J.C.K., J.R., and S.N.K. Funding acquisition: J.C.K. and J.R. Project administration: J.C.K. and J.R. **Competing interests:** J.C.K. receives consulting fees or salary, and holds equity in Corner Therapeutics, Larkspur Biosciences, MindImmune Therapeutics, and Neumora Therapeutics. None of these relationships affected this study. The other authors declare that they have no competing interests. **Data and materials availability:** All data needed to evaluate the conclusions in the paper are present in the paper and/or the Supplementary Materials.

Submitted 15 October 2024
Accepted 3 February 2025
Published 7 March 2025
10.1126/sciadv.adt9027